ACS APPLIED MATERIALS & INTERFACES

www.acsami.org
Research Article

Nebulization of RNA-Loaded Micelle-Embedded Polyplexes as a Potential Treatment of Idiopathic Pulmonary Fibrosis

Joschka T. Müller,[§] Adrian P. E. Kromer,[§] Aysan Ezaddoustdar, Ioannis Alexopoulos, Katharina M. Steinegger, Diana Leidy Porras-Gonzalez, Otto Berninghausen, Roland Beckmann, Peter Braubach, Gerald Burgstaller, Malgorzata Wygrecka, and Olivia M. Merkel*

Cite This: ACS Appl. Mater. Interfaces 2025, 17, 11861−11872
Read Online

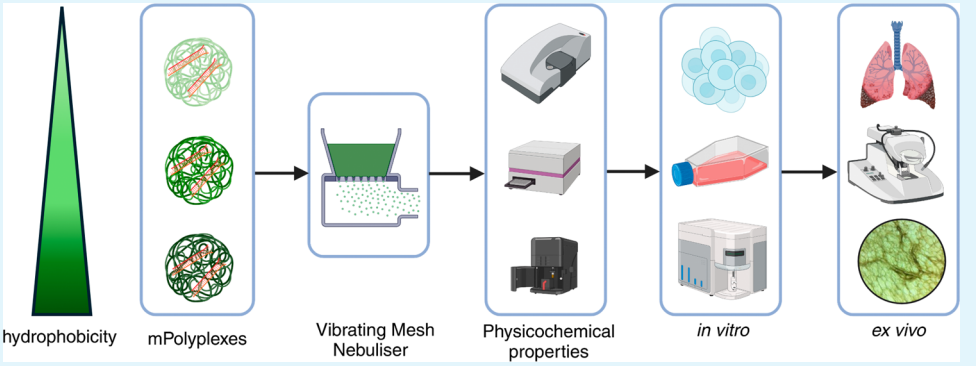

ABSTRACT: Biodegradable poly(β-amino) esters (PBAEs) have been a focus of interest for delivering therapeutic siRNA for several years. While no approved therapies are on the market yet, our study aims to advance PBAE-based treatments for currently "undruggable" diseases. The PBAEs used in this study are based on a recently reported step-growth copolymerization, which results in polymers with a unique balance of lipophilicity and positive charge, thereby showcasing diverse properties. Upon incubation with siRNA, these PBAEs form a unique structure and topology, which we classify as a subtype of classical polyplex, termed "micelle-embedded polyplexes" (mPolyplexes). The impact of different nebulizers on the physicochemical performance of these nanoparticles was investigated, and it was found that various mPolyplexes can be nebulized using vibrating-mesh nebulizers without the loss of gene silencing activity nor a change in physicochemical properties, setting them apart from other nanoparticles such as marketed LNPs. Finally, their therapeutic application was tested *ex vivo* in human precision-cut lung slices from patients with lung fibrosis. mPolyplexes mediated 52% gene silencing of matrix metalloprotease 7 (MMP7) and a downstream effect on collagen I (Col I) with 33% downregulation as determined via qPCR.

KEYWORDS: *siRNA, PBAE, polyplex, micelleplex, micelle-embedded polyplex, vibrating-mesh nebulizer, idiopathic pulmonary fibrosis*

1. INTRODUCTION

The lung offers numerous advantages for local administration over systemic administration, particularly when diseases originate in the lungs. This noninvasive approach is generally more comfortable for patients than parenteral administration. It is essential to distinguish whether the treatment is intended for local or systemic effects; in the former case, the drug should remain in the lungs for as long as possible to maximize its effectiveness and minimize side effects. Furthermore, this approach ensures direct delivery to the target tissue and cells, while reduced protein concentration in the lungs minimizes adsorption effects that can lead to unpredictable changes in cellular uptake.[1] The reduced overall protein concentration typically correlates with a reduced nuclease concentration in the lungs, enhancing RNA stability for pulmonary delivery.[2]

This study focuses on the treatment of idiopathic pulmonary fibrosis (IPF), a lung disease that would clearly benefit from a local therapeutic approach. Small interfering RNA (siRNA) presents a promising method for downregulating mRNA associated with the disease utilizing the cell's own machinery. While ONPATTRO, the first siRNA drug, was approved in 2018, no siRNA-based therapies have so far been approved for pulmonary application. However, numerous studies are currently underway targeting extrahepatic application, reflect-

Received: December 10, 2024
Revised: January 24, 2025
Accepted: January 27, 2025
Published: February 12, 2025

ing a growing interest in this research area.[3] For the encapsulation of negatively charged siRNA molecules using nonviral carriers, a variety of materials and nanoparticles are available, including lipid nanoparticles (LNPs), lipoplexes, polyplexes, micelleplexes, lipid−polymer hybrid nanoparticles, gold nanoparticles, and others. Our group specializes in biodegradable and biocompatible poly(β-amino) esters (PBAEs), which irregularly alternate with spermine side chains for RNA-encapsulating and oleylamine side chains for hydrophobicity and fusogenicity.[4,5]

To produce an inhalable formulation from aqueous solutions, different nebulization devices are available. Besides air-jet and ultrasonic nebulizers, vibrating-mesh nebulizers (VMN) are the most recently developed technology. VMNs nebulize aqueous suspensions via extrusion through a thin vibrating perforated membrane driven by piezoelectric crystals. Given that siRNA is an expensive and highly shear- and heat-sensitive material, it is essential to nebulize this active pharmaceutical ingredient (API) through the least stress-inducing nebulizer device. VMNs are suitable for this purpose due to their low dead volume, heat resistance, and low shear stress. Unsurprisingly, most current clinical trials of siRNA inhalation utilize VMNs.[6]

Here, we will evaluate two VMNs, the Aerogen Pro and the PARI eFlow Rapid, for their suitability in nebulizing PBAE-based drug delivery systems. Kleemann et al. described that VMNs are preferable to air-jet nebulizers for liposomal formulations due to lower shear stress.[7] VMNs also exert less thermal load, as the energy required for nebulization is introduced through the vibrating mesh rather than directly into the solution. Other researchers also identified VMNs as the best option for surface-active substances, as they maintained constant drug output.[8] However, the PARI eFlow Rapid caused a temperature increase of over 10 °C, as shown by Hertel et al., which is noticeably higher than the temperature increase of 3.2 °C for the Aerogen Pro.[9] Nevertheless, the same study demonstrated that active cooling prevented any temperature rise for over 4 min for the PARI eFlow Rapid. Furthermore, VMNs were shown to preserve the aerodynamic properties of reconstituted, freeze-dried nanoparticle suspensions during nebulization.[10] Unlike air-jet and ultrasonic nebulizers, which left most resuspended nanoparticles in the reservoir, VMNs did not. As a result, VMNs are recommended for "sensitive" formulations, including nanoparticle suspensions. Patel et al. further demonstrated that PBAE nanoparticles remain stable during nebulization with an Aerogen VMN, as evidenced by both dynamic light scattering (DLS) and electron microscopy (EM), resulting in uniform distribution across all five lung lobes after nebulization *in vivo*.[11]

IPF is clinically characterized by exertional dyspnea, dry cough, and often auscultatory findings, with a poor median survival of 3−5 years.[12,13] IPF pathogenesis is still poorly understood, but the prevailing theory involves repeated microinjuries to a genetically predisposed alveolar epithelium, followed by activation of fibroblasts, their transdifferentiation into collagen-producing myofibroblasts, and finally excessive extracellular matrix (ECM) deposition in the lungs.[14] This process impairs gas exchange and lung function. The accumulation of the ECM and Col I, a key component of a fibrotic ECM, creates a diffusive barrier that complicates treatment, a hallmark of all interstitial lung diseases. Interestingly, Jacquemart et al. demonstrated that hydrophobic materials exhibit stronger adsorption to Col I than more hydrophilic ones, a factor that could influence the effectiveness and penetration of PBAE formulations through collagen deposits in treating IPF.[15,16]

With IPF's unclear etiology, recent research has focused on identifying both genetic factors involved in the disease development and biomarkers with predictive, diagnostic, or prognostic value.[14] The only approved drugs for IPF, pirfenidone and nintedanib, have limited efficacy in reducing mortality, merely slowing disease progression through pleiotropic effects such as reducing inflammation and inhibiting fibroblast proliferation and ECM production.[17] Consequently, IPF is currently considered an "undruggable" disease, making it a prime candidate for siRNA-based interventions, which are commonly more target-specific than small-molecule drugs.

MMP7, a zinc-dependent endopeptidase, has been consistently identified as one of the most upregulated genes in the lungs of patients with various forms of progressive pulmonary fibrosis, including IPF.[17] Primarily expressed in lung epithelial cells, MMP7 (also known as matrilysin) contributes to IPF progression via the WNT/β-catenin pathways. Following the dephosphorylation of β-catenin, transcription factors are activated,[12] resulting in the transactivation of MMP7 and triggering downstream disease-promoting effects: MMP7 facilitates epithelial-to-mesenchymal cell transdifferentiation and increases profibrotic mediators through regulation of PKA and ERK1/2 signaling, ultimately leading to an overexpression of collagen I.[18,19] Elevated MMP7 levels have been found in lung tissues, the bronchoalveolar lavage fluid (BALF), and peripheral blood of IPF patients, with higher blood levels predicting increased mortality risk.[20] Notably, *in vivo* studies also suggest MMP7's central role, as $MMP7^{-/-}$ mice were protected against bleomycin-induced IPF.[21] Arrowhead Pharmaceuticals is currently conducting a clinical trial on inhaled siRNA targeting MMP7, underscoring its potential therapeutic application.[3]

The aim of this project is the development of an inhalable siRNA formulation for MMP7 downregulation. This aim was pursued by synthesizing various PBAEs with differing oleylamine (OA) contents and forming mPolyplexes by adding siRNA. Additionally, the impact of nebulization using VMNs on the stability and performance of these complexes was investigated, followed by testing in a relevant *ex vivo* model to downregulate the therapeutic target MMP7 using RNA interference (RNAi).

2. MATERIALS AND METHODS

2.1. Materials. Dicer substrate double-stranded siRNA targeting enhanced green fluorescent protein (eGFP) (siGFP, 25/27mer), amine-modified Dicer substrate double-stranded siRNA targeting enhanced green fluorescent protein (25/27mer), and scrambled siRNA (siNC, 25/27mer) were purchased from IDT (Integrated Technologies, Inc., Leuven, Belgium), and sequences and additional information are given in the Supporting Information, Table S1. HEPES (4-(2-hydroxyethyl)-1-piperazineethanesulfonic acid), Tris-EDTA buffer solution 100×, RPMI 1640 medium, Triton X-100, heparin sodium salt from porcine intestinal mucosa, heat-inactivated fetal bovine serum (FBS), penicillin/streptomycin solution (P/S), geneticin (G418), Dulbecco's phosphate-buffered saline (PBS), and branched polyethyleneimine (PEI) (5 kDa, Lupasol G100) were obtained from Sigma-Aldrich (Darmstadt, Germany). Di-*tert*-butyl decarbonate, oleylamine, spermine, Lipofectamine 2000, OPTI-MEM serum reduced medium, 0.05% trypsin-EDTA, Alexa Fluor 647 NHS

https://doi.org/10.1021/acsami.4c21657
ACS Appl. Mater. Interfaces 2025, 17, 11861−11872

ester, and a SYBR Gold Nucleic Acid Gel Stain 10.000X concentrate in DMSO and siMMP7 were purchased from Thermo Fisher Scientific (Schwerte, Germany). 1,4-Butanendiol diacrylate was obtained from TCI Chemical Industry Co., Ltd. (Tokyo, Japan). Trifluoroacetic acid (99,9%, extra pure) was purchased from Acros Organics (Geel, Belgium).

2.2. Polymer Synthesis. PBAE copolymers were synthesized applying a well-characterized synthesis approach previously reported by our group.[4] Briefly, the reaction was composed of a diacrylate monomer forming the backbone of the polymer and two side chains forming primary amines in different ratios. We applied 1,4-butandiol diacrylate as the backbone and tribocspermine (TBS) together with OA in different ratios. All educts were dissolved in a concentration of 300 mg/mL in DMF. After the reaction time, polymers were deprotected using trifluoroacetic acid. The deprotected polymers were precipitated three times in pentane before the final drying. Monomer ratios (stated forthgoing as the percentage of OA in the final polymer) were estimated by ^{1}H NMR spectroscopy.

2.3. Particle Preparation. Particles were prepared by using a batch mixing approach. Briefly, siRNA and polymer solutions were prepared and mixed in equivalent volumes of 10 mM HEPES at pH 5.4. Polymer concentrations varied between each polymer, and siRNA solutions were prepared at a concentration of 500 nM. PBAE or PEI was mixed with the siRNA solution by rapid pipetting for a defined speed and time. PBAE or PEI solutions were prepared at concentrations resulting in a 10-fold excess of protonated amines in the used polymer over phosphate groups in the siRNA backbone (N/P ratio of 10) following eqs 1 and 2.

$$\frac{N}{P} = \frac{m_{(\text{Polymer})}}{n_{(\text{siRNA})} \times n_{(\text{Nucleotides})} \times M_{(\text{Protonable Unit})}} \quad (1)$$

$$M_{(\text{Protonable Unit})} = \frac{(m_{(\text{OA})} \times r_{(\text{OA})}) + (m_{(\text{Spermine})} \times r_{(\text{Spermine})})}{(n_{(\text{OA amines})} \times r_{(\text{OA})}) + (n_{(\text{Spermine amines})} \times r_{(\text{Spermine})})} \quad (2)$$

where $m_{(\text{Polymer})}$ describes the mass of the used polymer, $n_{(\text{siRNA})}$ describes the molar amount of applied siRNA, $n_{(\text{Nucleotides})}$ is the molar amount of nucleotides in the used siRNA sequence, $r_{(\text{OA/Spermine})}$ gives the relative ratio of either OA or spermine in the used polymer, and $n_{(\text{OA/Spermine amines})}$ refers to the total number of protonable amines in the respective unit. After mixing, solutions were incubated at room temperature for 90 min for mPolyplexes (PBAE) and 30 min for polyplexes (PEI).

2.4. Nebulization. Two commercially available nebulizers were utilized for this study: a PARI eFlow Rapid (PARI, Starnberg, Germany) and an Aerogen Pro (Aerogen, Ratingen, Germany). Each nanoparticle suspension was immediately nebulized after the incubation time ended. Samples were loaded in the corresponding reservoirs, and aerosols were collected in cooled 15 mL Falcon tubes for further analysis. A minimum volume of 600 μL was applied to the Aerogen Pro and at least 1000 μL was added to the PARI eFlow Rapid for each nebulization.

2.5. Particle Characterization. The hydrodynamic diameter and polydispersity index (PDI) of nanoparticles were determined by dynamic light scattering (DLS), and the ζ-potential was determined by phase analysis light scattering (PALS) applying a Zetasizer Advance Ultra (Malvern Instruments, Inc., Malvern, UK) at a 173° backscatter mode. Nanoparticles were measured in formulation triplicates (N = 3) and analyzed using ZS Xplorer software (v.3.2.0). Additionally, nanoparticle tracking analysis (NTA) was applied using a NanoSight NS300 (Malvern Instruments, Inc., Malvern, UK) to support DLS data and obtain more information regarding particle concentration. All results are reported as the mean size (nm) ± the standard deviation (SD). Results were further validated using cryogenic transmission electron microscopy (cryo-TEM) of nanoparticle suspensions before and after nebulization.

2.6. RNA Encapsulation and Stability Assay. The RNA encapsulation efficiency was determined using a modified SYBR Gold assay, comparable to a previously described method.[22] Briefly, nanoparticles were prepared as described above and split before being partially subjected to nebulization. The collected samples were diluted with RNase-free water to obtain the same siRNA concentration as that in the RNA stability test. Formulations were transferred to a Fluotrac 384 well plate (Greiner Bio-One, Frickenhausen, Germany) and incubated for 1 h at 37 °C under shaking. Per sample, 3 μL of a 4× SYBR Gold Nucleic Acid Gel Stain was added and incubated for 5 min under light exclusion. The encapsulation efficiency was determined in comparison to a sample with siRNA only (non-nebulized), which represents 100% free siRNA. To evaluate potential losses of RNA through nebulization, a newly developed particle disruption approach was applied. Nanoparticles encapsulating 10 pmol of siRNA were prepared as described above and subjected to nebulization. Formulations were transferred to a Fluotrac 384 well plate. Per formulation, 10 μL of a 2% Triton X detergent solution and 2 μL of a 2000 U/mL heparin solution were added and incubated for 1 h at 37 °C under shaking. Subsequently, 3 μL of a 4× SYBR Gold Nucleic Acid Gel Stain was added and incubated for 5 min under light exclusion. A sample containing free siRNA only was subjected to the same conditions and represents 100% free siRNA. Following incubation, fluorescence measurements were conducted on a microplate reader (TECAN Spark, TECAN, Männedorf, Switzerland) at an excitation wavelength of 492/20 nm and an emission wavelength of 537/20 nm. The results are expressed as a percentage of free siRNA ± the standard deviation (SD). Technical triplicates (n = 3) of formulation triplicates (N = 3) were utilized for the measurements.

2.7. Molecular Dynamics Simulations. Molecular Dynamics (MD) simulations were run in Gromacs 2021.4 applying the Martini 3 force field as previously described.[23] The siRNA was adapted from the model introduced previously for the Martini 2 force field, whereas polymers were newly parametrized based on an all-atom model.[23]

Simulations contain 15 siRNA molecules and the respective polymer at an N/P ratio of 10, randomly inserted at the initial setup. The box size was (40 nm)^3, and molecules were solvated with 10 mM HEPES pH 5.4.

2.8. Aerosol Characterization by Laser Diffraction. Aerosol characterization was evaluated applying laser diffraction analysis. Particles were prepared as described above and nebulized with the two respective VMNs into the laser diffractor (HELOS, Sympatec, Clausthal-Zellerfeld, Germany) with an equipped R2 lens and INHALER module. Aerosol was applied through a punched silicone mouthpiece using an Aerogen Pro T-piece placed approximately 50−100 mm before entering the laser beam. The whole experimental setup was carried out in a closed Plexiglass box to control the relative humidity (% RH), which was kept over 70% RH during analysis. Aerosol was extracted at a rate of 13.9 L/min to avoid re-entry of aerosol to the laser beam. Each measurement consisted of three repeated runs with a duration of 5 s and a signal integration time of 200 ms. Measurements were carried out in triplicates (n = 3). Results are given as the Q3 volume median diameter (Q3-VMD) ± SD of nebulized droplets following the Mie theory suitable for nebulized droplets, calculated as an aqueous buffer with corresponding complex refractive indices.

2.9. *In Vitro* Protein Knockdown in H1299-eGFP Cells. H1299 cells stably expressing eGFP (H1299-eGFP) were used to determine the *in vitro* performance of the different nanoparticle systems. H1299-eGFP were cultured in an RPMI 1640 medium supplemented with 10% FBS, 1% P/S, and 0.4% G418. Cells were routinely cultured and passaged when reaching a confluency of 80−90% with 0.05% (v/v) trypsin and maintained at all times in humidified air with 5% CO_2 at a temperature of 37 °C. For experiments, cells were seeded at a density of 8×10^3 cells/well in 500 μL of a culture medium in 24-well plates and incubated for 24 h. Subsequently, the medium was exchanged, and transfection was performed by adding 100 μL of a transfection medium. The transfection medium consisted of nanoparticle suspensions encapsulating 50 pmol of siRNA either in a nebulized or non-nebulized form, 10 mM HEPES pH 5.4 as a blank, and free siRNA or Lipofectamine

https://doi.org/10.1021/acsami.4c21657
ACS Appl. Mater. Interfaces 2025, 17, 11861−11872

2000 with the same amount of siRNA, prepared according to the instruction manuals. Samples were prepared as described under Section 2.3 and were nebulized with the nebulizer, which had resulted in the lowest impact on physicochemical properties of the respective formulation. Following transfection, the cells were incubated for another 48 h. Afterward, cells were detached using 0.05% (v/v) trypsin and washed twice with PBS (400 rcf, 5 min, 21 °C) before resuspending them in 400 μL of PBS with 2 mM EDTA. Samples were analyzed by flow cytometry (Attune NxT, Thermo Fischer Scientific, Waltham, Massachusetts, USA), the average median fluorescence intensity (MFI) was measured with a 488 nm excitation laser, and emitted light was detected through the BL-1H filter set. Experiments were performed in three biological replicates (N = 3), each measured in technical triplicates (n = 3). Sample results are displayed as % eGFP expression through dividing the average MFI of siRNA-treated samples by blank samples with corresponding standard deviation (SD).

2.10. Application in Fibrotic Precision-Cut Lung Slices (PCLS). *2.10.1. Human Donors and Ethics Statement.* Investigations using a human fibrotic tissue were approved by the ethics committee of the Hannover Medical School (MHH, Hannover, Germany) and are in compliance with "The Code of Ethics of the World Medical Association" (renewed on 2015/04/22, number 2701-2015). Informed consent was obtained from all patients prior to their inclusion in the study. PCLS were prepared from explanted peripheral lung tissues obtained from 45- and 53-year-old male patients with progressive pulmonary fibrosis having a usual interstitial pneumonia (UIP) pattern. A nonfibrotic tissue from a non-CLD patient was obtained from the CPC-M bioArchive at the Comprehensive Pneumology Center (CPC Munich, Germany). The study was approved by the local ethics committee of the Ludwig-Maximilians-Universität of Munich, Germany (ethic vote 19-630). Written informed consent was obtained for the study participant.

2.10.2. Preparation of PCLS. After cannulating the human lung lobes with a flexible catheter, the explanted lung segments were inflated with warm (37 °C) low-melting agarose (1.5%) prepared in Dulbecco's modified Eagle's medium nutrient mixture F-12 Ham (DMEM-F-12), supplemented with 15 mM HEPES, 100 U/mL penicillin, and 100 μg/mL streptomycin (Invitrogen Life Technologies, Carlsbad, CA). Following the sol−gel transition of the agarose solution on ice, tissue cores of a diameter of 8 mm were sectioned into 250−300 μm thin slices using a sharp, rotating metal tube. The sectioning procedure was conducted using a Krumdieck Live Tissue Microtome (Alabama Research and Development, AL). PCLS were washed three times for 30 min in DMEM-F-12 supplemented with 15 mM HEPES, 100 U/mL penicillin, and 100 μg/mL streptomycin (growth medium) and then left for 2 days in culture to acclimate and settle prior to transfection experiments.

2.10.3. Transfection and MMP7 Gene Silencing in PCLS. PCLS were placed into a 12-well plate and cultured in 800 μL of a growth medium for 24 h. mPolyplexes were prepared according to Section 2.3 encapsulating either siMMP7, siNC, or Alexa Fluor 647-labeled siRNA at an N/P ratio of 10. Afterward, the mPolyplexes were nebulized applying the best suited nebulizer, and aerosol was collected in a 15 mL Falcon tube. Subsequently, PCLS were transfected with 100 pmol of siRNA in 200 μL of a formulation buffer. PCLS were cultured for another 72 h and then collected for imaging and RNA or protein isolation.

2.10.4. Two-Photon Laser Scanning Microscopy of PCLS. Two-photon microscopy of transfected PCLS was performed with an inverted Leica SP8 DIVE system, equipped with a SpectraPhysics Insight X3 multiphoton laser and external spectral detectors. For the acquisition of the two-photon z-stacks, we used a 10× 0.4 NA air objective, while the samples were mounted on a 35 mm glass-bottom dish with a glass thickness of 0.17 mm. The xyz image data had a voxel of 0.76 μm × 0.76 μm × 5 μm. The second harmonic generation (SHG), which was produced by collagen fibers, was acquired by using an excitation at 860 nm. The backscattered SHG was recorded with a Hybrid external spectral detector (HyD) set at the 425−430 nm detection range. Simultaneously, we recorded with a second HyD the autofluorescence signal (produced by the same excitation at 860 nm) in the range of 450−510 nm. The Alexa Fluor 647 dye was excited in a frame-by-frame sequential manner by a two-photon laser tuned at 1250 nm, and the emission was captured with an external spectral PMT (photomultiplier tube) at a range of 635−705 nm. The acquired image data were uploaded on an Omero instance, and the presented image panel was generated using the Omero.Figure plugin.[24]

2.10.5. RNA Isolation and qPCR. Total RNA was isolated by means of the TRIzol/chloroform method and quantified using a Nanodrop spectrophotometer (Thermo Fisher Scientific, Darmstadt, Germany). Complementary DNA (cDNA) was synthesized using a high-capacity cDNA reverse transcription kit (Thermo Fisher Scientific) according to the manufacturer's protocol. Quantitative real-time PCR (qRT-PCR) was performed using an iTaq Universal SYBR Green Supermix (Bio-Rad, Feldkirchen, Germany) on a StepOnePlus system (Thermo Fisher Scientific). Hypoxanthine guanine phosphoribosyltransferase (HPRT) was used as the reference gene. For normalization of MMP7 levels, the ΔΔCt method was applied. The primer sequences used are depicted in Table 1.

Table 1. Primers for the PCR Reaction[a]

name	primer sequences (5′−3′)
MMP7	Fw: AGTGAGCTACAGTGGGAACAG
	Rev: TTTTGCATCTCCTTGAGTTTGGC
HPRT	Fw: AAGGACCCCACGAAGTGTTG
	Rev: GGCTTTGTATTTTGCTTTTCCA
collagen I	Fw: CTCCCCAGCCACAAAGAGTC
	Rev: CCGTTCTGTACGCAGGTGAT
fibronectin	Fw: CACCTCTGTGCAGACCACAT
	Rev: ACCACACCACTGTCTGTGAC

[a]A = Adenine; C = cytosine; G = guanine; T = thymine; MMP7 = matrix metalloprotease-7; HPRT = hypoxanthine guanine phosphoribosyltransferase; Fw = forward; Rev = reverse.

2.10.6. Western Blotting. PCLS were homogenized in a lysis buffer containing 50 mM Tris (pH 7.4), 150 mM NaCl, 1 mM EDTA, 1% Triton X-100, 1% sodium deoxycholate, and 0.1% SDS, supplemented with 1 mM Na_3VO_4, 1 mM PMSF protease inhibitor, and 1 μg/mL cOmplete protease inhibitor cocktail (Roche Applied Science, Indianapolis, IN). The detergent-insoluble material was precipitated by centrifugation at 18,600g for 30 min at 4 °C. The protein concentration was measured using a Pierce BCA protein assay kit (Thermo Fisher Scientific). Twenty μg of protein was separated on a 12% SDS polyacrylamide gel and subsequently transferred to a PVDF membrane (Roth, Karlsruhe, Germany). The membrane was blocked with 5% nonfat milk for 1 h at room temperature and then incubated with a mouse anti-MMP7 (1:500, cat. no. MAB9071, R&D Systems, Wiesbaden, Germany) or goat anticollagen 1 (1:500, cat. no. 1310-01, SouthernBiotech, Birmingham, AL) antibody overnight at 4 °C. β-actin, used as a loading control, was detected using a mouse anti-β-actin antibody (1:5000, cat. no. A1978, Sigma-Aldrich, Taufkirchen, Germany). Proteins were detected using either an Amersham ECL Select Western blotting detection reagent (GE Healthcare, Chicago, IL) or a Pierce ECL Western blotting substrate (Thermo Fisher Scientific). All images were acquired using a ChemiDoc imaging system (Bio-Rad, Hercules, CA).

2.11. Statistical Analysis. All experiments were performed in triplicates. Statistical analysis was performed using GraphPad Prism 9.5.1 software and one-way ANOVA analysis or an unpaired t test.

3. RESULTS AND DISCUSSION

3.1. Particle Formation. Using the endogenous polyamine spermine, we established polymers with significantly improved encapsulation efficiencies, reaching 100% encapsulation at polymer:siRNA weight ratios of less than 10. It was previously

https://doi.org/10.1021/acsami.4c21657
ACS Appl. Mater. Interfaces 2025, 17, 11861−11872

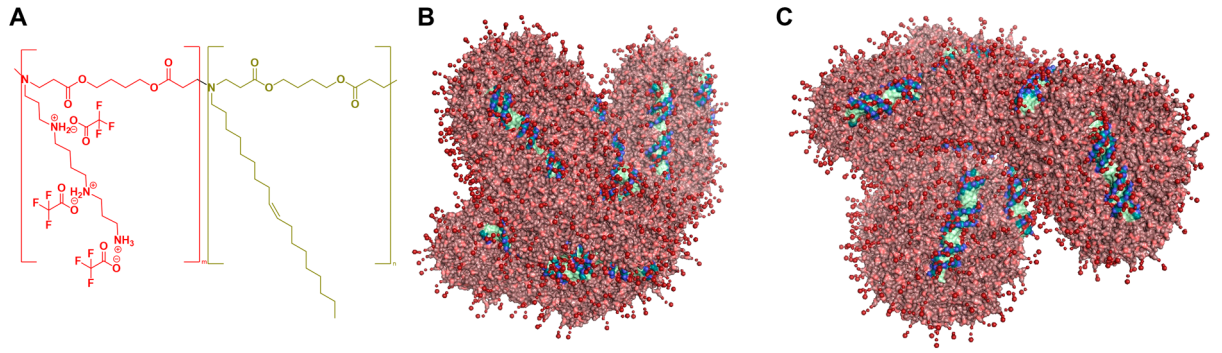

Figure 1. (A) Chemical structure of the PBAEs described here with ionic spermine (red) and hydrophobic oleylamine (brown) side chains; (B,C) two projections of MD simulations of mPolyplexes made of the 75% OA polymer at an N/P 10 and a pH of 5.4 in a 10 mM HEPES buffer. Green and blue structures depict siRNA strands, light red structures represent the hydrophobic parts of the polymer, and dark red spots denote the hydrophilic spermine subunits.

shown that introducing hydrophobicity into polymeric siRNA delivery vehicles can have many advantages, such as increasing transfection efficiency through enhanced endosomal escape[5] and reducing toxicity through shielding of cationic charges.[25,26] Therefore, we introduced varying hydrophobicity into the PBAE polymers studied here in a new and precise matter applying a controlled synthesis approach previously reported by our lab (Figure 1A).[4] This enabled a precise tuning of polymer characteristics, improving the conclusiveness of the resulting data. By analyzing the resulting structures with various methods, including cryo-TEM and MD simulations, a new structure type of nanoparticle was observed and named micelle-embedded polyplexes. This name was chosen because of the results obtained by previous MD simulations showing a deviation from typical micelleplex or polyplex structures reported by our group.[23] Micelleplexes are known to have a hydrophobic core and a hydrophilic shell in which the siRNA is encapsulated. Polyplexes such as PEI typically have a uniform inner structure composed of encapsulated siRNA and a polymer. Our results indicate the formation of small micelles composed of the PBAE carrier attached to the siRNA with their hydrophilic outer shell. Thereby, larger structures form with an siRNA core, a hydrophobic micelle-shell, and a hydrophilic outer surface, composed of spermine side chains. Several of these structures coalesce into bigger particles with an additional hydrophilic outer shell (Figure 1B,C). Due to this unique structure, we named these particles micelle-embedded polyplexes (mPolyplexes).

3.2. Particle Characterization. The aim of this study was therapeutic pulmonary delivery of siRNA to target idiopathic pulmonary fibrosis. Therefore, a suitable delivery route to reach the cytosol of alveolar cells was necessary. As already discussed above, VMNs have been reported to be the gentlest aerosolization devices for liquid formulations. Here, the two clinically applied VMNs, the PARI eFlow Rapid and the Aerogen Pro, were applied to nebulize different mPolyplex suspensions. The difference between non-nebulized and nebulized particles was investigated for each mPolyplex formulation nebulized with each VMN. For additional comparison, PEI polyplexes were nebulized and investigated as well (Figure 2A).

All polymers tested formed monodisperse particles with a small size ranging from 90 to 110 nm and a PDI of 0.1−0.2 (Figure 2B). The 30% OA mPolyplexes formed the smallest and the 75% OA mPolyplexes formed the largest particles. This size increase may be due to decreased charge density in the 75% OA mPolyplexes, leading to less compact particles. As the OA ratio increases, particle hydrophobicity also rises, leading to a greater proportion of weaker hydrophobic interactions as particle stabilizing forces. Consequently, the overall intraparticular forces decrease, potentially causing larger particles, as was similarly observed with NTA (Figure 2C). All particles exhibited positive ζ-potentials between 15 and 25 mV (Figure 2D), crucial for cellular uptake as the positive charge aids in attraction to the negatively charged cellular membrane,[27] which is rich in glycan chains. Although not statistically significant, the ζ-potential decreased with increasing OA ratios, likely due to shielding effects of the hydrophobic polymer content. Finally, the siRNA encapsulation and release from the particles were evaluated, and all polymers encapsulated 100% of the provided siRNA at an N/P of 10, with no detectable free siRNA even after nebulization. Interestingly, only a combination of Triton X, a surfactant that disrupts hydrophobic interactions, and heparin, a polyanion that displaces siRNA from polyplexes through competition, successfully released 100% of the encapsulated siRNA from the mPolyplexes (Figure 2E,F). Neither heparin nor Triton X alone achieved full siRNA release (data not shown, but available in this reference[22]). This observation suggests that mPolyplexes are stabilized by hydrophobic and electrostatic intraparticular forces, which underlines the unique structure of this new particle class.

PEI and 30% OA mPolyplexes showed no statistically significant changes in their physicochemical properties after nebulization with either VMN. Parameters such as the hydrodynamic diameter (Figure 2B), PDI (Figure 2B), particle concentration (Figure 2C), and ζ-potential (Figure 2D) remained stable, indicating that the stronger ionic intraparticular forces are resistant to nebulization-associated stress. Changes were only observed for particles with a higher hydrophobicity content. Physicochemical characteristics of 55% OA mPolyplex were affected by nebulization with the PARI eFlow Rapid. The hydrodynamic diameter increased (Figure 2B), while the particle concentration, determined by NTA, decreased (Figure 2C). This concentration drop likely results from aggregate formation during nebulization, explaining the increased particle size. A similar, though not statistically significant, trend was observed for the 30% OA mPolyplexes (Figure 2C), suggesting that higher hydrophobic contents within the particles increase the susceptibility to VMN-induced shear stress. Interestingly, this susceptibility was even more pronounced in the 75% OA mPolyplex, but only when

https://doi.org/10.1021/acsami.4c21657
ACS Appl. Mater. Interfaces 2025, 17, 11861−11872

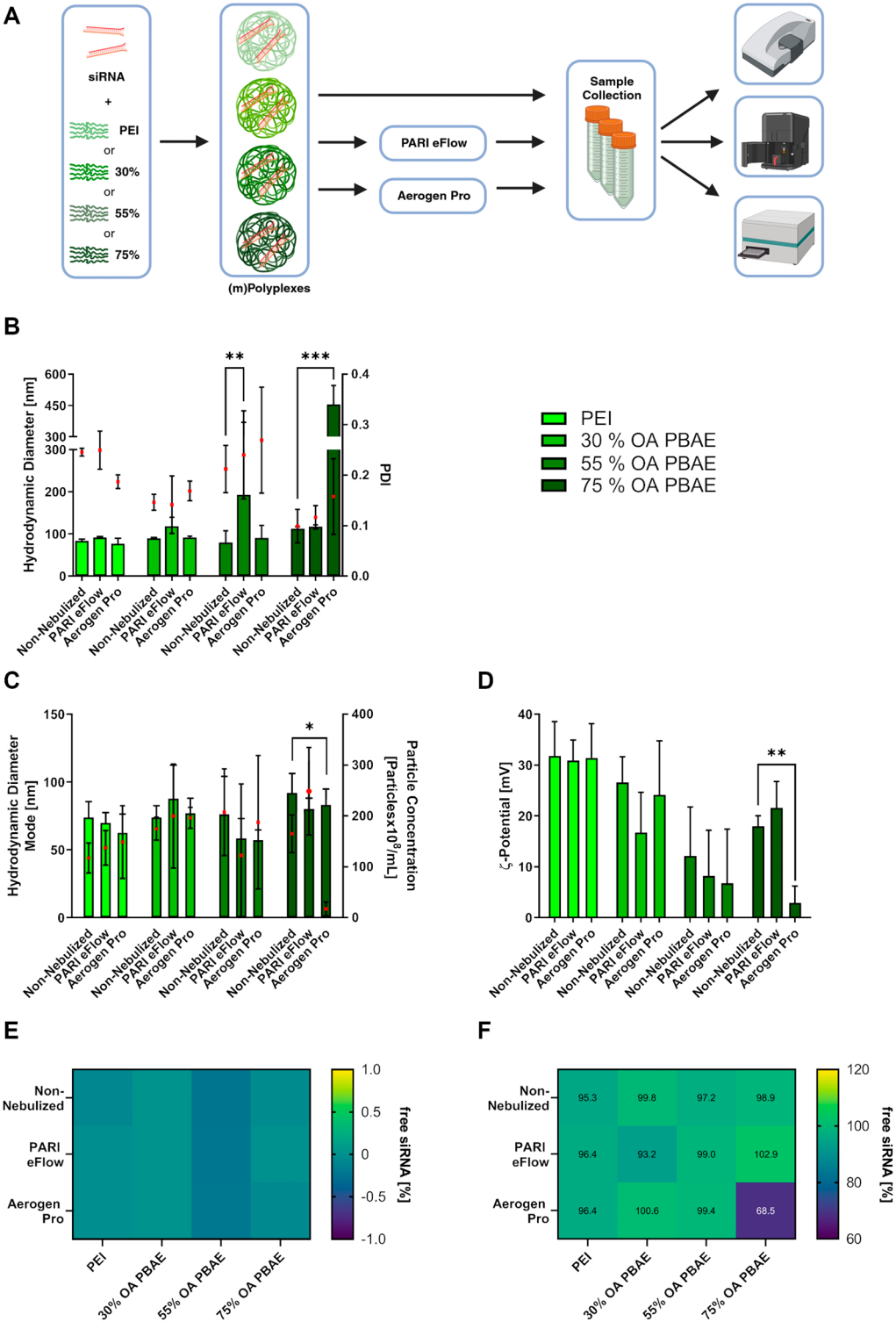

Figure 2. Physicochemical characteristics of PEI polyplexes and mPolyplex formulations before and after nebulization with two different nebulizers. (A) Scheme describing the experimental workflow and (B) hydrodynamic diameter, determined via DLS with a 173° backscatter angle in a bar graph and the polydispersity index (PDI) as red dots in the same graph, with the color legend present on the right side. The color legend also serves for (C) and (D). Statistical analysis refers to hydrodynamic diameter data. (C) Mode of the particle sizes [nm] and the particle concentration in 10^8 particles/mL determined by nanoparticle tracking analysis. Statistical analysis refers to particle concentration data. (D) ζ-Potential determined by phase analysis light scanning. (E) [%] Encapsulated siRNA, either in a non-nebulized state or nebulized via the two respective VMNs; (F) [%] released siRNA, either in a non-nebulized state or nebulized via the two respective VMNs. Error bars denote means ± SD (N = 3); one-way ANOVA, *p < 0.05, **p < 0.01, ***p < 0.001, and no indication reflects nonsignificant differences.

nebulized with the Aerogen Pro VMN. Here, the hydrodynamic diameter increased significantly (Figure 2B), and the ζ-potential became significantly more neutral (Figure 2D), which could promote aggregation due to reduced particle

https://doi.org/10.1021/acsami.4c21657
ACS Appl. Mater. Interfaces 2025, 17, 11861−11872

repulsion. This explains the increased particle size and significantly lower particle concentration (Figure 2C). Additionally, these particles were the only formulation in which only a fraction of the encapsulated siRNA could be recovered (Figure 2F). It remains unclear if the siRNA was indeed degraded or if the formed aggregates resisted complete dissociation by the Triton X and heparin mixture.

It seems plausible that the higher OA content, with its weaker intracellular forces, the 55% OA mPolyplexes, was insufficient to withstand the higher energy input of the PARI eFlow Rapid (Table 2). However, it is surprising that this trend

Table 2. Differences in Performance-Indicating Parameters for the PARI eFlow Rapid and Aerogen Pro VMNs

nebulizer	energy input [J/g][28]	nebulization speed [mL/min]	residual volume [mL]
PARI eFlow Rapid	35 ± 12	0.54	∼1
Aerogen Pro	18 ± 6	0.29	n. a.

was not observed in the 75% OA mPolyplexes, which appeared more resistant to the high energy input but were more sensitive to the faster nebulization speed. This suggests that the shear stress in the Aerogen Pro may be higher, causing destabilization of the 75% OA mPolyplexes.

These results confirm that a suitable VMN device was identified for all mPolyplex formulations, without impacting their physicochemical characteristics. Cryo-TEM images of the 30 and 55% OA mPolyplexes taken before and after nebulization (Figure S1) further support this observation. It was concluded that particles stabilized by hydrophobic interactions are more susceptible to nebulizer-induced aggregation and degradation, a trend also observed with lipid nanoparticles. However, it is surprising that mPolyplexes with very high OA ratios responded differently to the two tested nebulizers.

3.3. Aerosol Characterization by Laser Diffraction.

Aerosol characterization was carried out using laser diffraction, with results presented as Q3-VMD in Table 3. The results

Table 3. Laser Diffraction Results of Different Nebulized Nanoparticle Formulations[a]

sample	X (Q3 = 50%) [μm] Aerogen Pro	X (Q3 = 50%) [μm] PARI eFlow Rapid
10 mM HEPES	5.43 ± 0.09	4.49 ± 0.13
PEI	4.54 ± 0.07	4.77 ± 0.06
30% OA PBAE	4.19 ± 0.01	4.12 ± 0.16
55% OA PBAE	4.31 ± 0.04	4.19 ± 0.09
75% OA PBAE	4.18 ± 0.02	4.25 ± 0.11

[a]Data points indicate means ± SD, n = 3.

allow a direct comparison of each nanoparticle formulation, varying in the hydrophobic content, across the different VMNs in comparison with the formulation buffer only. PEI served as the control for siRNA polyplexes without any surface-active properties.

As shown in Table 3 and Figure S2, all nebulized nanoparticle formulations fell within the 1−5 μm droplet range, a well-known size range for effective sedimentation and deposition within the alveoli, making all tested nebulizers suitable for pulmonary delivery of the chosen formulations.[29] An interesting trend emerged for the Aerogen Pro: the formulation buffer only showed the highest median diameter at 5.43 ± 0.09 μm. When PEI polyplexes were added, the median diameter decreased to 4.54 ± 0.07 μm. However, including surface-active polymers forming mPolyplexes further reduced the median diameter, with the 75% OA PBAE (the most lipophilic compound) reaching a minimum of 4.18 ± 0.02 μm with the Aerogen Pro.

A similar trend was observed with the PARI eFlow, though less pronounced: the formulation buffer had a median diameter of 4.49 ± 0.13 μm, which increased slightly to 4.77 ± 0.06 μm with PEI polyplexes. However, adding amphiphilic nanoparticles reduced the median diameter below that of the formulation buffer, reaching a low of 4.12 ± 0.16 μm for the 30% OA PBAE polyplex formulation.

The literature provides some theories about these findings: first, adding nanoparticles to the buffer may decrease the median droplet diameter due to higher charge density from negatively charged siRNA and positively charged carriers, such as PEI and PBAEs. Increased charge density is known to reduce the mass median aerodynamic diameter (MMAD), as shown in studies adding different salts to nebulizer solutions.[30,31] Zhang et al. observed that increased conductivity lowers the droplet VMD and fine particle fraction (FPF) of aerosols and increases reproducibility between the measurements.[31]

The experimental setup chosen here also answers the less clear question of the influence of surface-active molecules on aerosol characteristics. Studies with surfactants, such as SDS (sodium dodecyl sulfate) and Tween 20, in formulations used in vibrating-mesh nebulizers resulted in a decrease in VMD. Beck-Broichsitter et al. attributed this effect primarily to the increased conductivity rather than changes in surface tension alone, as both parameters were monitored during their study.[32]

A 2012 study found that increasing poly(vinyl alcohol) (PVA) concentrations reduced MMAD,[10] suggesting that surface-active molecules significantly affect droplet size. According to Tate's law, surface tension influences the droplet volume as Zhang et al. noted.[31] Another factor is the wetting of the hydrophilic nebulizer's palladium−nickel membrane. While increased surface tension reduces output due to decreased spreading on the nebulizer membrane, Zhang et al. also found that surfactants such as pluronic at equilibrium concentrations cannot consistently lower surface tension at the continuously forming new droplet interfaces. The comparably minor influence of surface tension was explained by the surfactants' slow adsorption rate to the newly created air−water interfaces, leading to surface tension gradients at the site where aerosol droplets form.[31]

It was also shown that increased viscosity reduces MMADs and output ranges,[30] but this parameter is expected to have little-to-no influence here. Instead, the relative humidity significantly impacts aerosol performance, with higher % RH (as present in the physiological lung) leading to smaller median diameters, fitting better into the target 1−5 μm range. This is due to the faster evaporation from smaller particles at low % RH leading to a shift to wrongfully higher median diameters. Therefore, our experimental setup (Figure S3) was all enclosed in a plastic box with a humidifier (Beurer GmbH, Ulm, Germany), maintaining values above 70% RH.

3.4. *In Vitro* Protein Knockdown in H1299-eGFP Cells.

Although the above experiments showed that the physicochemical properties of the nanoparticle systems remained stable during nebulization with at least one of the tested

https://doi.org/10.1021/acsami.4c21657
ACS Appl. Mater. Interfaces 2025, 17, 11861−11872

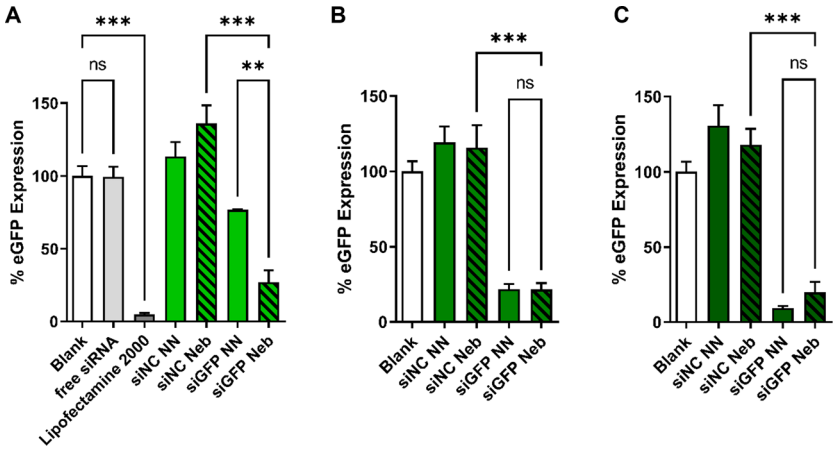

Figure 3. *In vitro* eGFP knockdown in H1299-eGFP cells. Polymers with varying OA contents encapsulating 50 pmol siRNA were tested either in non-nebulized (NN) or in a nebulized (Neb) form and compared to blank cells (white bar), free siRNA (light gray,) and Lipofectamine 2000 lipoplexes encapsulating the same siRNA as the positive control (dark gray). mPolyplexes are divided into (A) 30% OA PBAE, (B) 55% OA PBAE, and (C) 75% OA PBAE. Bars show % eGFP expression as calculated from MFI values ± SD ($N = 3$); one-way ANOVA, $^{**}p < 0.01$, $^{***}p < 0.001$, and ns = nonsignificant.

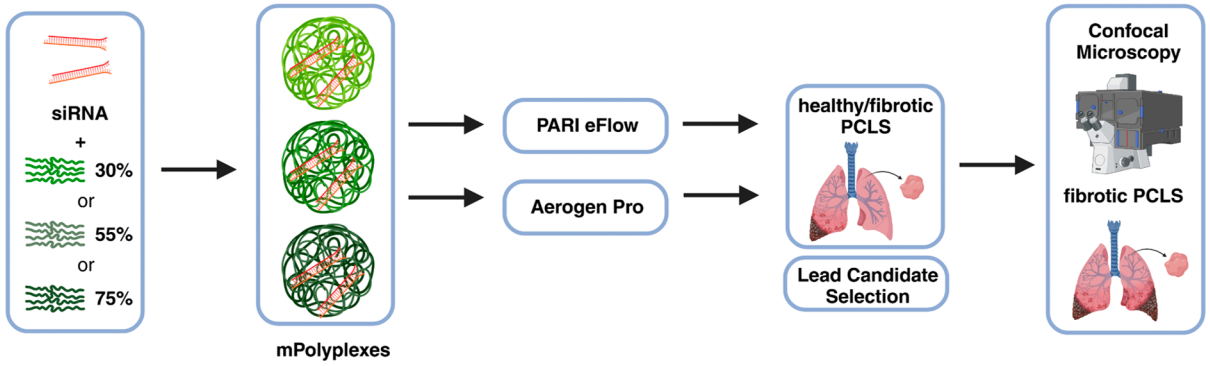

Figure 4. Workflow of NP's performance evaluation *ex vivo*. The siRNA was encapsulated by 30, 55, and 75% OA PBAE polymers at an N/P of 10 and nebulized via the Pari eFlow Rapid or Aerogen Pro and evaluated in healthy and/or fibrotic PCLS.

VMNs, it is equally important to preserve the biological stability and activity of the siRNA during this process. To assess biological activity postnebulization, the stably eGFP expressing cell line H1299-eGFP served as an *in vitro* model for siRNA gene silencing efficacy. This epithelial-like lung cell line is an ideal model as it mimics the likely port of entry for nebulized formulations.

Based on the above experiments, the best-performing nebulizers were selected for each formulation: the Aerogen Pro for 30% OA PBAE and 55% OA PBAE mPolyplexes was chosen and the PARI eFlow Rapid for 75% OA PBAE mPolyplexes. As shown in Figure 3A–C, particles encapsulating negative control siRNA had no gene silencing efficacy at all. On the contrary, these particles seemed to induce eGFP, possibly through nanoparticle-stimulated overall induction of protein biosynthesis. Most importantly, however, siGFP-loaded nanoparticles mediated sequence-dependent RNAi: the 30% OA non-nebulized mPolyplexes reduced eGFP expression by about 23% (Figure 3A), while the nebulized achieved a 73% reduction, tripling gene silencing efficacy despite no observable differences in physicochemical properties. Nebulization was hypothesized to induce internal structural changes that may loosen siRNA/polymer interactions. A previously reported stability assay confirmed this assumption (Figure S4), revealing a decrease in EC_{50} from 9.4 to 8.4, indicating slightly weakened intraparticular forces. It was previously hypothesized that highly stable particles can be detrimental to successful cytosolic siRNA delivery due to a hampered release of siRNA.[33] It is important to point out that the reduced intraparticular binding strength had no observable impact on the colloidal stability. Additionally, no significant differences in transfection efficiency were observed between non-nebulized and nebulized 55% OA PBAE (Figure 3B) and 75% OA PBAE formulations (Figure 3C). In the case of the most cationic 30% OA PBAE polymer (Figure 3A), however, significantly improved gene silencing activity after nebulization further supports our hypothesis of a reduction in intraparticular binding strength during nebulization.

Comparing the three different OA contents of the PBAEs reveals a trend: a higher hydrophobic OA content correlates with increased gene silencing efficacy. The 75% OA PBAE mPolyplexes showed the highest efficiency, silencing eGFP by 91% in the non-nebulized form and 80% postnebulization. The 55% OA PBAE achieved 78% before and 79% after nebulization. The recent literature also underlines this trend,[4,5] suggesting that a higher unsaturated fatty acid content enhances nanoparticle fusogenicity, thus enhancing endosomal escape. Furthermore, considering the changed behavior of the 30% OA PBAE before and after nebulization, it is possible that increased hydrophobic contents could lead to a favorable less

https://doi.org/10.1021/acsami.4c21657
ACS Appl. Mater. Interfaces 2025, 17, 11861−11872

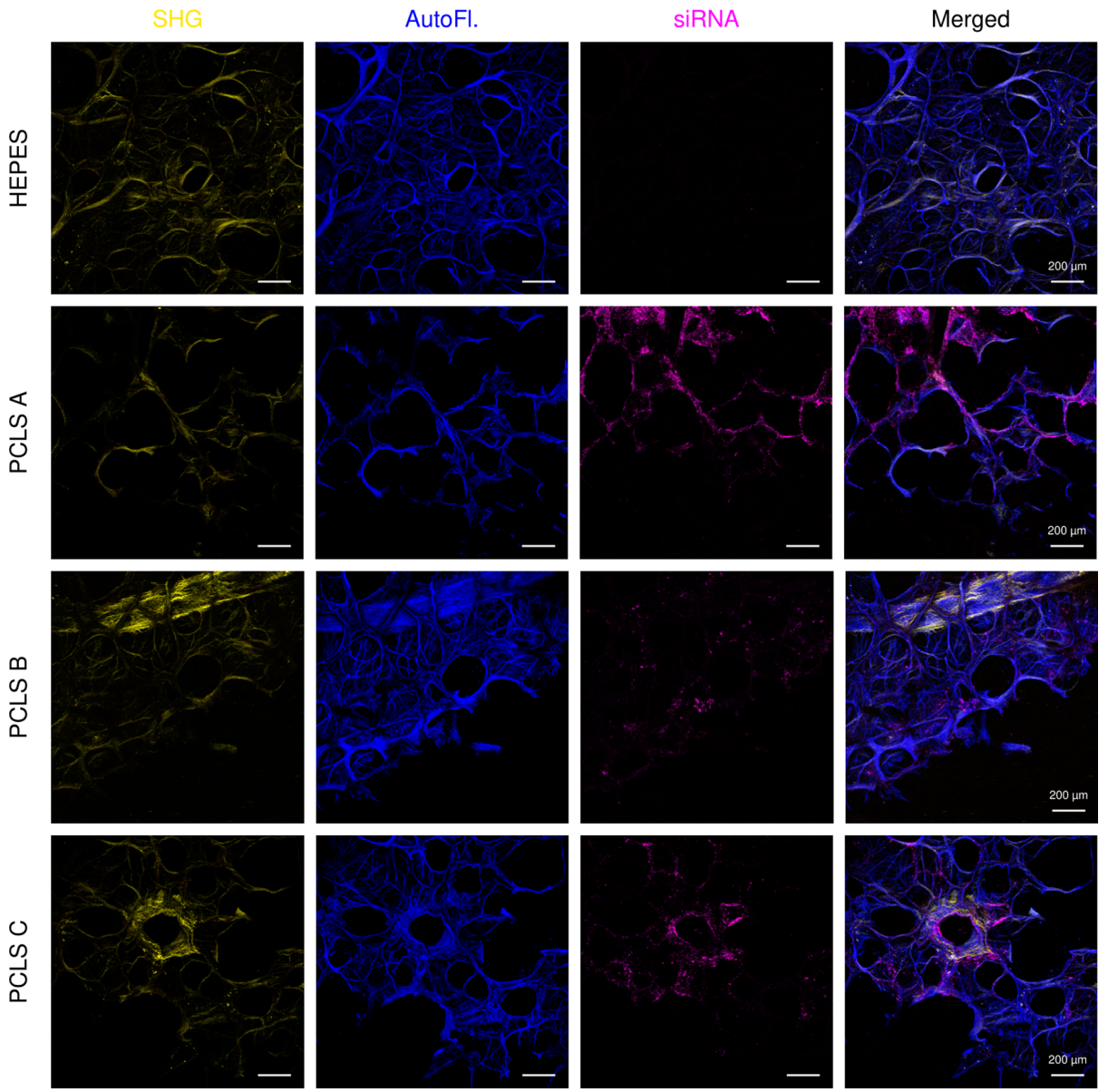

Figure 5. Maximum intensity projections of two-photon microscopy images of fibrotic PCLS; the first column presents the second harmonic generation (SHG in yellow) from collagen fibers, the second column presents tissue autofluorescence in blue (450−510 nm), the third column shows the signal of Alexa Fluor 647 (in magenta), while the last column is an overlay of all channels. The first row indicated as HEPES was transfected with 10 mM HEPES, pH 5.4 as a blank; PCLS A, B, and C were transfected with 100 pmol of AF-647-labeled siRNA, encapsulated by 30% OA PBAE at an N/P ratio of 10.

pronounced siRNA binding to the polymer, allowing more effective siRNA release. Overall, these results are promising for therapeutic applications, as the biological effect of mPolyplexes was maintained or even improved after nebulization.

3.5. Nanoparticle Transfection Efficiency in Fibrotic PCLS. Following the 3R principle, we applied a model better suited for studying human IPF than classical murine models. We tested the efficacy of our approach in the complex model of human lung fibrosis using PCLS, which maintain the lung's native architecture, including cell and ECM composition, and thus mimic the disease's pathophysiological characteristics (Figure 4).[34] Studying nanoparticle behavior in this diseased state is crucial for better understanding potential treatment options and advancing from preclinical to clinical stages. Preliminary experiments in peritumor tissues, using GAPDH knockdown, showed no difference between the nebulized and non-nebulized 30% OA PBAE mPolyplexes (Figure S5). In fact, mPolyplexes made of 30% OA PBAE showed no negative changes in the physicochemical properties across all VMNs. While mPolyplexes made of 75% OA PBAE showed a slight decrease in gene silencing efficacy postnebulization, the 30% OA PBAE mPolyplexes performed better in PCLS (Figure S5). Furthermore, initial prescreening in fibrotic PCLS showed superior gene silencing capacity of the 30% OA PBAE in comparison to the more lipophilic ones (Figure S6), making it the lead candidate for additional PCLS experiments.

The transfection efficacy of this lead formulation was subsequently investigated in three PCLS samples from different regions of the fibrotic lung from one patient using high-resolution live imaging. A transfection control with only formulation buffer was included. As shown in Figure 5, all PCLS samples displayed a pronounced ECM, visualized by

https://doi.org/10.1021/acsami.4c21657
ACS Appl. Mater. Interfaces 2025, 17, 11861−11872

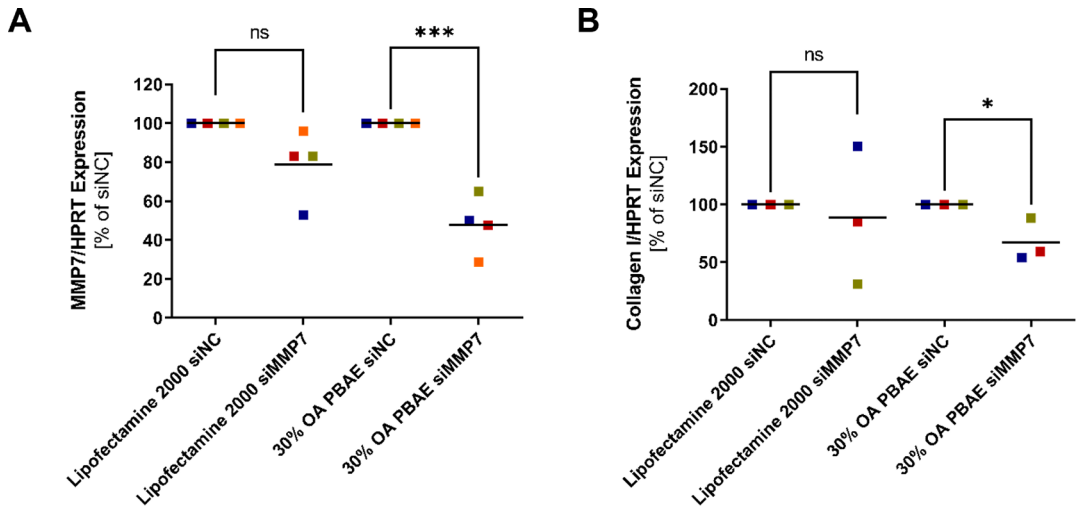

Figure 6. *Ex vivo* MMP7 knockdown in fibrotic PCLS. Fibrotic PCLS were transfected with 100 pmol of either siMMP7 or siNC, encapsulated by 30% OA PBAE, with an N/P of 10, after nebulization or with the same amount of siRNA lipoplexes, formed with Lipofectamine 2000 as the positive control. RT-qPCR results from (A) MMP7 and (B) collagen I in comparison to the housekeeping gene HPRT. Unpaired *t* test, $*p < 0.05$, $***p < 0.001$, and ns = nonsignificant. Dots indicate results from each single fibrotic tissue, while the line indicates the mean ($N = 4$ for (A) and $N = 3$ for (B)).

strong fluorescence in the second harmonic generation (SHG) channel, which visualizes fibrillar collagen I and II, confirming the fibrotic nature of the samples. In the control sample with HEPES, no fluorescence was detected in the siRNA channel, but strong fluorescence appeared in all nanoparticle-treated samples, indicating excellent transfection efficiency with varying signal intensity depending on lung tissue architecture and cell composition. Across all three *ex vivo* samples, the siAF647-labeled nanoparticles penetrated the fibrotic PCLS, confirming that excessive collagen in the model does not hinder nanoparticle mobility.

3.6. MMP7 Knockdown in a Relevant Idiopathic Fibrotic PCLS Model. The gene silencing efficacy of mPolyplexes was further investigated in a relevant idiopathic fibrotic PCLS model. MMP7, a profibrotic molecule that contributes to increased ECM production and, consequently, to elevated collagen I levels, is a promising RNAi target for treating IPF. Given the satisfactory siRNA delivery efficiency observed in confocal images, 30% OA mPolyplexes were selected to assess the MMP7 knockdown potential. Lipofectamine 2000, while efficient for transfection, is too toxic for *in vivo* use and served as a positive control only. According to qPCR results (Figure 6A), using the ΔΔCt method with the housekeeping gene HPRT, Lipofectamine 2000 achieved a relative knockdown of 21% of the target gene compared to siNC samples. Interestingly, the nebulized lead nanoparticle formulation showed a superior 52% knockdown, surpassing Lipofectamine 2000's transfection level without its associated high toxicity. For the downstream effect, collagen I levels were determined via qPCR, showing similar trends (Figure 6B): while Lipofectamine 2000 treatment led to a nonsignificant gene silencing of 11%, the tested 30% OA PBAE achieved a downregulation of 33% for Col I, indicating that the MMP7 downstream cascade was partially inhibited *ex vivo*. Fibronectin levels, which are also considered to be part of IPF's pathology,[35] were downregulated on minor levels for Lipofectamine 2000 and 30% OA PBAE after siMMP7 treatment and are depicted in Figure S5.

Interestingly, the hydrophobic carrier appears to influence the treatment effectiveness. Others have shown that hydrophobic polystyrene exhibits stronger adsorption to collagen I than its oxidized counterpart.[15] Therefore, it is hypothesized that 30% OA PBAE mPolyplexes balance effective collagen penetration with sufficient endosomal release for gene silencing. While increasing the OA content improved knockdown efficiency in the H1299-eGFP model before nebulization, this effect was less pronounced in peritumoral PCLS tissues (Figures S6 and S7). Consequently, it can be inferred that in tissues with significant collagen overexpression, the use of a more hydrophilic carrier system may be advantageous.

Western blot analysis was used to assess the effect of the siRNA formulations on protein levels, specifically targeting MMP7 (Figure S8), with β-actin serving as a control protein. 30% OA mPolyplexes reduced MMP7 protein levels compared to the control formulation, leading to a marked reduction in collagen I expression, a downstream effector of MMP7. Since collagen I is a key ECM component and is often elevated in IPF patients, this reduction is highly relevant and suggests that this treatment may positively influence the progression of the disease, addressing the underlying cause of IPF rather than merely alleviating symptoms.

Therefore, the primary advantages of these newly developed PBAE-micelleplexes lie in their excellent nebulizability, which retains or even enhances their functionality, as well as their customizable properties. The ability to adjust the lipophilic content to suit specific disease states is particularly advantageous, as is the overall flexibility in modifying structural entities and potentially incorporating targeting ligands.

4. CONCLUSIONS

This study demonstrated that PBAE-based nanoparticles can be nebulized using clinically relevant VMNs without altering their physicochemical characteristics. Increasing hydrophobicity reduced nanoparticle stability against nebulization associated stress, but suitable nebulization settings were found to maintain particle integrity and functionality as confirmed *in vitro*. The presence of mPolyplexes slightly decreased the

https://doi.org/10.1021/acsami.4c21657
ACS Appl. Mater. Interfaces 2025, 17, 11861−11872

VMDs of buffer solutions with the used VMNs. The research aimed to assess a potential inhalable siRNA therapeutic approach for IPF. With a disease-relevant *ex vivo* model, successful nanoparticle uptake and MMP7 gene knockdown were confirmed via Western blotting and qPCR in PCLS, resulting in downregulation of the disease-related protein collagen I. These findings highlight the potential of this new delivery system for targeting pulmonary diseases, even in challenging conditions such as IPF. Especially, the tunability of hydrophobicity and nebulizer settings allows for rapid adaptation to different pathophysiological needs. Furthermore, IPF patients would benefit from nebulization as a route of administration compared to other pulmonary delivery methods such as pressurized metered dose inhalers or dry powder inhalers due to their often limited lung capacity. Additionally, this approach could also be applied to other pulmonary diseases, including asthma or chronic obstructive pulmonary disease, by choosing a suitable molecular target. It is believed that this study will advance nebulization-based pulmonary disease research and accelerate the development of clinically relevant formulations.

■ ASSOCIATED CONTENT

Supporting Information

The Supporting Information is available free of charge at https://pubs.acs.org/doi/10.1021/acsami.4c21657.

siRNA sequences used in this research, cryo-TEM micrographs of freshly prepared and nebulized mPolyplexes, laser diffraction results of nebulized formulations, photograph of the experimental setup within an equipped humidity box, mPolyplex stability data before and after nebulization, gene silencing results in human peritumor and fibrotic lung tissues, and Western blot analysis results (PDF)

■ AUTHOR INFORMATION

Corresponding Author

Olivia M. Merkel − *Department of Pharmacy, Ludwig-Maximilians-Universität Munich, 81377 Munich, Germany; Center for NanoScience (CeNS), Ludwig-Maximilians-Universität Munich, 80799 Munich, Germany; Ludwig-Maximilians-Universität Munich, Member of the German Center for Lung Research (DZL), 81377 Munich, Germany;* orcid.org/0000-0002-4151-3916; Email: olivia.merkel@lmu.de

Authors

Joschka T. Müller − *Department of Pharmacy, Ludwig-Maximilians-Universität Munich, 81377 Munich, Germany*

Adrian P. E. Kromer − *Department of Pharmacy, Ludwig-Maximilians-Universität Munich, 81377 Munich, Germany*

Aysan Ezaddoustdar − *Center for Infections and Genomics of the Lung (CIGL) Justus Liebig University Giessen German Center for Lung Research, 35392 Gießen, Germany*

Ioannis Alexopoulos − *Center for Infections and Genomics of the Lung (CIGL) Justus Liebig University Giessen German Center for Lung Research, 35392 Gießen, Germany; Institute of Lung Health (ILH), Justus Liebig University Giessen, 35392 Gießen, Germany*

Katharina M. Steinegger − *Department of Pharmacy, Ludwig-Maximilians-Universität Munich, 81377 Munich, Germany;* orcid.org/0009-0002-3396-9654

Diana Leidy Porras-Gonzalez − *Comprehensive Pneumology Center with the CPC-M bioArchive and Institute of Lung Health and Immunity, Helmholtz-Zentrum München, Member of the German Center of Lung Research (DZL), 81377 Munich, Germany*

Otto Berninghausen − *Department of Biochemistry, Gene Center, Ludwig-Maximilians-Universität Munich, 81377 Munich, Germany*

Roland Beckmann − *Department of Biochemistry, Gene Center, Ludwig-Maximilians-Universität Munich, 81377 Munich, Germany*

Peter Braubach − *Biomedical Research in Endstage and Obstructive Lung Disease Hannover (BREATH) Research Network, Member of the German Center for Lung Research (DZL), Hannover Medical School, 30625 Hanover, Germany*

Gerald Burgstaller − *Comprehensive Pneumology Center with the CPC-M bioArchive and Institute of Lung Health and Immunity, Helmholtz-Zentrum München, Member of the German Center of Lung Research (DZL), 81377 Munich, Germany*

Malgorzata Wygrecka − *Center for Infections and Genomics of the Lung (CIGL) Justus Liebig University Giessen German Center for Lung Research, 35392 Gießen, Germany*

Complete contact information is available at: https://pubs.acs.org/10.1021/acsami.4c21657

Author Contributions

[§]J.T.M. and A.P.E.K. contributed equally to this work.

Notes

The authors declare no competing financial interest.

■ ACKNOWLEDGMENTS

We thank Ronan MacLoughlin from Aerogen Ltd. for kindly providing us the used Aerogen Pro for experimental purposes. Olivia Merkel gratefully acknowledges the Volkswagen Foundation (AZ-9A872) and the European Research Council (ERC-2022-COG-101088587). We gratefully acknowledge the provision of human biomaterial (nonfibrotic fresh tissue from a non-CLD patient) and clinical data from the CPC-M bioArchive and its partners at the Asklepios Biobank Gauting, the LMU Hospital, and the Ludwig-Maximilians-Universität München. We thank the patient and their family for their support. We thank Thomas Michler for providing scientific input and supervision. Figures were partially generated using biorender.com.

■ REFERENCES

(1) Hartl, N.; Jurgens, D. C.; Carneiro, S.; Konig, A. C.; Xiao, X.; Liu, R.; Hauck, S. M.; Merkel, O. M. Protein Corona Investigations of Polyplexes with Varying Hydrophobicity - from Method Development to in Vitro Studies. *Int. J. Pharm.* **2023**, *643*, No. 123257.

(2) Qiu, Y.; Lam, J. K.; Leung, S. W.; Liang, W. Delivery of Rnai Therapeutics to the Airways-from Bench to Bedside. *Molecules* **2016**, *21* (9), 1249.

(3) Guo, F.; Li, Y.; Yu, W.; Fu, Y.; Zhang, J.; Cao, H. Recent Progress of Small Interfering Rna Delivery on the Market and Clinical Stage. *Mol. Pharmaceutics* **2024**, *21* (5), 2081−2096.

(4) Kromer, A. P. E.; Sieber-Schafer, F.; Farfan Benito, J.; Merkel, O. M. Design of Experiments Grants Mechanistic Insights into the Synthesis of Spermine-Containing Pbae Copolymers. *ACS Appl. Mater. Interfaces* **2024**, *16* (29), 37545−37554.

(5) Jin, Y.; Wang, X.; Kromer, A. P. E.; Müller, J. T.; Zimmermann, C.; Xu, Z.; Hartschuh, A.; Adams, F.; Merkel, O. M. Role of Hydrophobic Modification in Spermine-Based Poly(Beta-Amino Ester)S for Sirna Delivery and Their Spray-Dried Powders for Inhalation and Improved Storage. *Biomacromolecules* **2024**, *7*, 4177−4191.
(6) Neary, M. T.; Mulder, L. M.; Kowalski, P. S.; MacLoughlin, R.; Crean, A. M.; Ryan, K. B. Nebulised Delivery of Rna Formulations to the Lungs: From Aerosol to Cytosol. *J. Controlled Release* **2024**, *366*, 812−833.
(7) Kleemann, E.; Schmehl, T.; Gessler, T.; Bakowsky, U.; Kissel, T.; Seeger, W. Iloprost-Containing Liposomes for Aerosol Application in Pulmonary Arterial Hypertension: Formulation Aspects and Stability. *Pharm. Res.* **2007**, *24* (2), 277−287.
(8) Arzhavitina, A.; Steckel, H. Surface Active Drugs Significantly Alter the Drug Output Rate from Medical Nebulizers. *Int. J. Pharm.* **2010**, *384* (1−2), 128−136.
(9) Hertel, S.; Pohl, T.; Friess, W.; Winter, G. That's Cool!–Nebulization of Thermolabile Proteins with a Cooled Vibrating Mesh Nebulizer. *Eur. J. Pharm. Biopharm* **2014**, *87* (2), 357−365.
(10) Beck-Broichsitter, M.; Kleimann, P.; Schmehl, T.; Betz, T.; Bakowsky, U.; Kissel, T.; Seeger, W. Impact of Lyoprotectants for the Stabilization of Biodegradable Nanoparticles on the Performance of Air-Jet, Ultrasonic, and Vibrating-Mesh Nebulizers. *Eur. J. Pharm. Biopharm* **2012**, *82* (2), 272−280.
(11) Patel, A. K.; Kaczmarek, J. C.; Bose, S.; Kauffman, K. J.; Mir, F.; Heartlein, M. W.; DeRosa, F.; Langer, R.; Anderson, D. G. Inhaled Nanoformulated Mrna Polyplexes for Protein Production in Lung Epithelium. *Adv. Mater.* **2019**, *31* (8), No. e1805116.
(12) Chanda, D.; Otoupalova, E.; Smith, S. R.; Volckaert, T.; De Langhe, S. P.; Thannickal, V. J. Developmental Pathways in the Pathogenesis of Lung Fibrosis. *Mol. Aspects Med.* **2019**, *65*, 56−69.
(13) Tomos, I.; Roussis, I.; Matthaiou, A. M.; Dimakou, K. Molecular and Genetic Biomarkers in Idiopathic Pulmonary Fibrosis: Where Are We Now? *Biomedicines* **2023**, *11* (10), 2796.
(14) El Agha, E.; Wygrecka, M. State of the Art in Idiopathic Pulmonary Fibrosis. *Cells* **2022**, *11* (16), 2487.
(15) Jacquemart, I.; Pamula, E.; De Cupere, V. M.; Rouxhet, P. G. C.; Dupont-Gillain, Ch Nanostructured Collagen Layers Obtained by Adsorption and Drying. *J. Colloid Interface Sci.* **2004**, *278* (1), 63−70.
(16) Dupont-Gillain, C. C. Understanding and Controlling Type I Collagen Adsorption and Assembly at Interfaces, and Application to Cell Engineering. *Colloids Surf. B Biointerfaces* **2014**, *124*, 87−96.
(17) Craig, V. J.; Zhang, L.; Hagood, J. S.; Owen, C. A. Matrix Metalloproteinases as Therapeutic Targets for Idiopathic Pulmonary Fibrosis. *Am. J. Respir. Cell Mol. Biol.* **2015**, *53* (5), 585−600.
(18) Chilosi, M.; Poletti, V.; Zamò, A.; Lestani, M.; Montagna, L.; Piccoli, P.; Pedron, S.; Bertaso, M.; Scarpa, A.; Murer, B.; et al. Aberrant Wnt/B-Catenin Pathway Activation in Idiopathic Pulmonary Fibrosis. *American Journal of Pathology* **2003**, *162* (5), 1495−1502.
(19) Ślusarz, A.; Nichols, L. A.; Grunz-Borgmann, E. A.; Chen, G.; Akintola, A. D.; Catania, J. M.; Burghardt, R. C.; Trzeciakowski, J. P.; Parrish, A. R. Overexpression of Mmp-7 Increases Collagen 1a2 in the Aging Kidney. *Physiological Reports* **2013**, *1* (5), 1−20.
(20) Rosas, I. O.; Richards, T. J.; Konishi, K.; Zhang, Y.; Gibson, K.; Lokshin, A. E.; Lindell, K. O.; Cisneros, J.; Macdonald, S. D.; Pardo, A.; et al. Mmp1 and Mmp7 as Potential Peripheral Blood Biomarkers in Idiopathic Pulmonary Fibrosis. *PLoS Med.* **2008**, *5* (4), No. e93.
(21) Zuo, F.; Kaminski, N.; Eugui, E.; Allard, J.; Yakhini, Z.; Ben-Dor, A.; Lollini, L.; Morris, D.; Kim, Y.; DeLustro, B.; et al. Gene Expression Analysis Reveals Matrilysin as a Key Regulator of Pulmonary Fibrosis in Mice and Humans. *Proc. Natl. Acad. Sci. U. S. A.* **2002**, *99* (9), 6292−6297.
(22) Carneiro, S. P.; Müller, J. T.; Merkel, O. M.Fluorescent Techniques for Rna Detection in Nanoparticles. In *Rna Amplification and Analysis: Methods and Protocols*, Astatke, M., Ed.; Springer: US, 2024; pp 187−203.
(23) Steinegger, K. M.; Allmendinger, L.; Sturm, S.; Sieber-Schäfer, F.; Kromer, A.; Müller-Caspary, K.; Winkeljann, B.; Merkel, O. M. Molecular Dynamics Simulations Lucidates the Molecular Organisation of Poly(Beta-Aminoester) Based Polyplexes for Sirna Delivery. *Nano Lett.* **2024**, 15683.
(24) Allan, C.; Burel, J.-M.; Moore, J.; Blackburn, C.; Linkert, M.; Loynton, S.; MacDonald, D.; Moore, W. J.; Neves, C.; Patterson, A.; et al. Omero: Flexible, Model-Driven Data Management for Experimental Biology. *Nat. Methods* **2012**, *9* (3), 245−253.
(25) Nelson, C. E.; Kintzing, J. R.; Hanna, A.; Shannon, J. M.; Gupta, M. K.; Duvall, C. L. Balancing Cationic and Hydrophobic Content of Pegylated Sirna Polyplexes Enhances Endosome Escape, Stability, Blood Circulation Time, and Bioactivity in Vivo. *ACS Nano* **2013**, *7* (10), 8870−8880.
(26) Ogris, M.; Brunner, S.; Schüller, S.; Kircheis, R.; Wagner, E. Pegylated DNA/Transferrin−Pei Complexes: Reduced Interaction with Blood Components, Extended Circulation in Blood and Potential for Systemic Gene Delivery. *Gene Ther.* **1999**, *6* (4), 595−605.
(27) Jeon, S.; Clavadetscher, J.; Lee, D. K.; Chankeshwara, S. V.; Bradley, M.; Cho, W. S. Surface Charge-Dependent Cellular Uptake of Polystyrene Nanoparticles. *Nanomaterials (Basel)* **2018**, *8* (12), 1028.
(28) van Rijn, C. J. M.; Vlaming, K. E.; Bem, R. A.; Dekker, R. J.; Poortinga, A.; Breit, T.; van Leeuwen, S.; Ensink, W. A.; van Wijnbergen, K.; van Hamme, J. L.; et al. Low Energy Nebulization Preserves Integrity of Sars-Cov-2 Mrna Vaccines for Respiratory Delivery. *Sci. Rep* **2023**, *13* (1), 8851.
(29) Ray, L.Chapter 4 - Polymeric Nanoparticle-Based Drug/Gene Delivery for Lung Cancer. In *Nanotechnology-Based Targeted Drug Delivery Systems for Lung Cancer*, Kesharwani, P., Ed.; Academic Press, 2019; pp 77−93.
(30) Ghazanfari, T.; Elhissi, A. M.; Ding, Z.; Taylor, K. M. The Influence of Fluid Physicochemical Properties on Vibrating-Mesh Nebulization. *Int. J. Pharm.* **2007**, *339* (1−2), 103−111.
(31) Zhang, G.; David, A.; Wiedmann, T. S. Performance of the Vibrating Membrane Aerosol Generation Device: Aeroneb Micropump Nebulizer. *J. Aerosol Med.* **2007**, *20* (4), 408−416.
(32) Beck-Broichsitter, M.; Knuedeler, M. C.; Seeger, W.; Schmehl, T. Controlling the Droplet Size of Formulations Nebulized by Vibrating-Membrane Technology. *Eur. J. Pharm. Biopharm* **2014**, *87* (3), 524−529.
(33) Abdul Ghafoor Raja, M.; Katas, H.; Jing Wen, T.; Ceña, V. Stability, Intracellular Delivery, and Release of Sirna from Chitosan Nanoparticles Using Different Cross-Linkers. *PLoS One* **2015**, *10* (6), No. e0128963.
(34) Cedilak, M.; Banjanac, M.; Belamaric, D.; Paravic Radicevic, A.; Faraho, I.; Ilic, K.; Cuzic, S.; Glojnaric, I.; Erakovic Haber, V.; Bosnar, M. Precision-Cut Lung Slices from Bleomycin Treated Animals as a Model for Testing Potential Therapies for Idiopathic Pulmonary Fibrosis. *Pulm Pharmacol Ther* **2019**, *55*, 75−83.
(35) Wygrecka, M.; Kwapiszewska, G.; Jablonska, E.; Gerlach, S. v.; Henneke, I.; Zakrzewicz, D.; Guenther, A.; Preissner, K. T.; Markart, P. Role of Protease-Activated Receptor-2 in Idiopathic Pulmonary Fibrosis. *Am. J. Respir Crit Care Med.* **2011**, *183* (12), 1703−1714.

https://doi.org/10.1021/acsami.4c21657
ACS Appl. Mater. Interfaces 2025, 17, 11861−11872